Int. J. Heat Mass Transfer. Vol. 28, No. 4, pp. 779-788, 1985
Printed in Great Britain

0017-9310/85 $3.00 + 0.00

A differential model for salt-stratified, double-diffusive systems heated from below

T. L. BERGMAN, F. P. INCROPERA and R. VISKANTA
Heat Transfer Laboratory, School of Mechanical Engineering, Purdue University, West Lafayette, IN 47907, U.S.A.

(*Received* 26 *June* 1984 *and in final form* 9 *October* 1984)

Abstract—A differential model is developed and used to predict the transient response of a salt-stratified, double-diffusive system heated from below. Predicted mixed layer heights and temperature distributions are in good agreement with data and in reasonable agreement with predictions based on simpler one- and two-layer models. Key features of the system, such as the substantial density difference across the interfacial boundary layer, negligible variation of the salinity profile in the stable region, and locations of highly anisotropic fluid motion are well described by the model. Predicted turbulence characteristics are plausible, and predicted mixed layer growth rates are consistent with accepted correlations involving a convective velocity and a mixed layer Richardson number.

INTRODUCTION

SALT-STRATIFIED solutions heated from below are characterized by vertical distributions of salt and temperature which are associated with stable and unstable density distributions, respectively. With two diffusing species (heat and salt) of nonuniform distribution, the density gradient at any location may induce convective motion, which strongly influences the temperature and salt profiles. Double-diffusive, thermohaline conditions are pertinent to natural phenomena, such as the thermohaline structure of the upper ocean [1], and to engineering problems such as the salt gradient solar pond [2], the storage of liquified natural gas [3], and crystal growth [4]. An understanding of double-diffusive system behavior is essential for reliable design or analysis of such systems.

When an initially isothermal, salt-stratified solution is heated from below, a potentially unstable temperature gradient develops above the heated surface. The temperature gradient may induce convective motion, which, unlike conditions for a single-diffusive fluid, is confined to a bottom mixed layer whose growth is inhibited by the stabilizing salt distribution. Mixed region growth is typically slow and occurs at the expense of the overlying stable region, as fluid is entrained through an interfacial boundary layer separating the two regions. Although the entrainment mechanism(s) are poorly understood, it is known that the transfer of turbulent kinetic energy from the mixed layer to the interfacial boundary layer is at least partially responsible for the entrainment [1]. A schematic of the salt-stratified solution heated from below, along with representative temperature and salinity profiles, is shown in Fig. 1.

For large values of the bottom heat flux and/or small stabilizing salt concentration gradients, bottom mixed layer growth may be curtailed when an unstable temperature distribution ahead of this layer induces a series of multiple mixed layers [5]. New layers may continue to form, while existing layers merge in lower regions of the system. In contrast, for small heat fluxes and/or large salinity gradients, slow growth of the bottom mixed layer occurs continuously, without multiple layer formation [6]. In the limit of very small heat fluxes and large salinity gradients, mixed layer formation may never occur.

Although there have been many experimental studies of thermohaline system behavior, little has been done to predict this behavior. The earliest model was developed by Turner [7], who used a lumped capacitance approach which neglected heat transfer from the mixed layer to the stable region. The model predicted the temporal variation of mixed layer height and temperature and provided good agreement with data for weekly stratified solutions heated vigorously from below. However, poor agreement was obtained for systems with moderate to large salt gradients and moderate to small heat fluxes [8]. The model was extended by Huppert and Linden [5], who included the

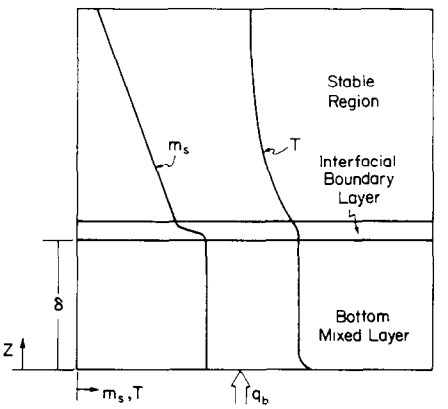

FIG. 1. Schematic of an initially isothermal, salt-stratified solution heated from below.

NOMENCLATURE

B	buoyancy parameter
c	specific heat [J kg^{-1} K^{-1}]
$c_{i\varepsilon}$	empirical constant, i = 1,2,3
c_μ	empirical constant
c_t'	empirical constant
D_{AB}	binary diffusion coefficient [m^2 s^{-1}]
f_2	empirical function
g	gravitational acceleration [m s^{-2}]
k	turbulence kinetic energy per unit mass [m^2 s^{-2}]
k	thermal conductivity [W m^{-1} K^{-1}]
L	arbitrary length [m]
m_s	average salt mass fraction
m_s'	fluctuating salt mass fraction
Pr	Prandtl number, $\mu c/k$
q_b	bottom heat flux [W m^{-2}]
Ra_s	solutal Rayleigh number, $(g\beta_s L^4 \partial m_s/\partial z)/(\alpha\nu)$
Ra_T^*	thermal Rayleigh number, $(g\beta_T q_b L^4)/(k\alpha\nu)$
Re_t	turbulence Reynolds number, $\rho k^2/(\mu\varepsilon)$
Ri	Richardson number, $g\Delta\rho\delta/(\rho u_*^2)$
Sc	Schmidt number, $\mu/(\rho D_{AB})$
T	average temperature [°C]
T'	fluctuating temperature [°C]
t	time [s]
u_e	entrainment velocity [m s^{-1}]
u_*	convective velocity [m s^{-1}]
w'	fluctuating vertical velocity [m s^{-1}]
X	relative stability parameter
z	vertical space coordinate positive upwards [m].

Greek symbols

α	thermal diffusivity
β_s	saline expansion coefficient [m^3 kg^{-1}]
β_T	thermal expansion coefficient [K^{-1}]
δ	mixed layer height [m]
ε	dissipation of turbulence kinetic energy per unit mass [m^2 s^{-3}]
μ	dynamic viscosity [kg m^{-1} s^{-1}]
ν	kinematic viscosity [m^2 s^{-1}]
ρ	density [kg m^{-3}]
$\Delta\rho$	density difference across the interfacial boundary layer [kg m^{-3}]
σ_k	turbulence kinetic energy Prandtl number
σ_ε	dissipation Prandtl number
ϕ, ϕ_t, ϕ_t'	empirical constants.

Subscripts

e	effective
i	initial
j	experiment number
min	minimum
s	saline
T	thermal
t	turbulent.

effects of heat transfer to the stable region and subsequent multiple mixed layer formation by using empirical correlations for heat and salt transport through thin diffusive interfaces separating mixed layers of different density [9]. However, applicability of the model is still restricted to small salinity gradients and large heat fluxes.

In an attempt to treat conditions for which heat loss to the diffusive region is significant, Bergman *et al.* [10] developed a multilayer model by applying species and energy balances to control volumes about the bottom mixed layer and the diffusive region. Entrainment rates were predicted from a correlation based on an overall mixed layer Richardson number [11]. Although the model predicts mixed layer height, temperature and salinity, it cannot predict local features of the system, such as distributions near the heated surface and within the interfacial boundary layer. Meyer [12] also proposed a model to determine mixed layer development in systems for which heat loss to the stable region is significant. The empirical formulae of Turner [9] were used to predict entrainment through the interfacial boundary layer. Although the model used a finite-difference scheme to solve differential formulations of the conservation equations, local phenomena were not reported.

Presently, there is clear need for a model which is without restrictive assumptions [5, 7], which is based on first principles and does not rely extensively on empirical information [10, 12], and which is capable of predicting local conditions. Also, there is need of experimental data covering a wide range of system behavior, with which resulting model predictions may be compared. Accordingly the primary objective of this study is to develop a model which is capable of predicting mixed layer growth, as well as local temperature, salinity, and density distributions in mixed, interfacial and stable layers, for salt-stratified solutions heated from below. Results of the model are compared with measured growth rates and temperature distributions obtained from a supporting experimental study.

MATHEMATICAL MODEL

As it expands due to entrainment at the interfacial boundary layer, flow conditions within a bottom-heated mixed layer are characterized by a random, three-dimensional convection pattern. If the convecting flow is turbulent, an appropriate turbulence model is needed to predict system behavior. Although many differential models could be used for this purpose, none have yet been used to predict double-diffusive system behavior.

Although expressions for the turbulent stresses and fluxes may be developed from a one-equation turbulence kinetic energy (k) model [13], use of such a model is precluded by lack of an empirical length scale distribution for the system of interest. The relevant length scale could be predicted from a two-equation (k–ε) model which uses an additional turbulence equation for the dissipation of turbulence kinetic energy (ε). However, the model is limited by its inability to predict individual Reynolds stresses and turbulence fluxes which result from the inherently anisotropic nature of turbulence in buoyancy driven systems [13, 14]. In addition, the k–ε model utilizes a gradient-based diffusion concept considered to be inapplicable for certain thermally driven systems [14].

To more accurately describe the turbulence, a stress/flux model [13], such as those which have been applied to the atmospheric boundary layer [15], could be specified. However, in addition to presenting formidable numerical difficulties (models with up to 28 coupled equations have been proposed [13]), modeling of higher order terms in the stress/flux equation is still in the developmental stage, even for extensively studied systems such as the atmospheric boundary layer [16]. Moreover, while solution of the stress/flux model would enhance the detail to which system turbulence is predicted, such detail is well beyond that which has been determined experimentally in double-diffusive systems. Finally, although new subgrid models may be used to determine spectral characteristics of turbulent fluctuations [17], the models are limited by closure problems and have enormous computational requirements [13, 17].

Since the lack of empirical information concerning length scale distributions or distributions of higher order fluxes precludes the use of simpler or more complex turbulence models, the k–ε turbulence model was chosen for this study. It should be noted, however, that the study is not an attempt to combine turbulence modeling with experimental results to validate closure hypotheses. Instead, it constitutes a first attempt to predict relevant experimental results, such as mixed layer heights and temperature distributions, by using an existing turbulence model. Indeed, it has been recently observed [18] that turbulent systems of this nature (diffusion of grid-generated turbulence into a stably stratified fluid) constitute yet another type of flow well-suited for calibration of all turbulence models including, specifically, the k–ε model. Although the particular formulation of the k–ε model used in this study is unable to predict anisotropic behavior or the existence of coherent structures, inclusion of these effects is believed to be premature, until experimental results providing detailed individual turbulence values or coherent structures become available.

Since the flow is randomly three-dimensional, several simplifying assumptions must be made to effect a solution. Energy transfer is assumed to be one-dimensional, and contributions due to species diffusion and diffusion thermo are neglected. Similarly, species transfer is assumed to be one-dimensional, and thermal diffusion is neglected, since it may be shown that salt transport by this process is negligible for the system of interest [19]. Internal waves and the fluctuation of solution properties are also neglected. Mean thermophysical properties are allowed to vary since such variation is considerable for saline water solutions [20].

The energy and species equations are of the form

$$\frac{\partial}{\partial t}(\rho cT) = \frac{\partial}{\partial z}\left(\frac{\mu c}{Pr}\frac{\partial T}{\partial z}\right) - \frac{\partial}{\partial z}(\rho c\overline{w'T'}) \tag{1}$$

$$\frac{\partial}{\partial t}(\rho m_s) = \frac{\partial}{\partial z}\left[\frac{\mu}{\rho Sc}\frac{\partial}{\partial z}(\rho m_s)\right] - \frac{\partial}{\partial z}(\rho\overline{w'm_s'}) \tag{2}$$

where the two terms on the RHS of each equation account for transfer by molecular and turbulent diffusion. Introducing turbulent exchange coefficients to relate the turbulent diffusion terms to local temperature and salt concentration gradients [13]

$$\rho c\overline{w'T'} = -\frac{c\mu_t}{Pr_t}\frac{\partial T}{\partial z} \tag{3}$$

$$\rho\overline{w'm_s'} = -\frac{\mu_t}{\rho Sc_t}\frac{\partial(\rho m_s)}{\partial z} \tag{4}$$

and defining effective parameters of the form

$$\mu_e = \mu + \mu_t \tag{5}$$

$$Pr_e = \mu_e/(\mu/Pr + \mu_t/Pr_t) \tag{6}$$

the energy and species equations may be expressed as

$$\frac{\partial}{\partial t}(\rho cT) = \frac{\partial}{\partial z}\left(\frac{\mu_e}{Pr_e}c\frac{\partial T}{\partial z}\right) \tag{7}$$

$$\frac{\partial}{\partial t}(\rho m_s) = \frac{\partial}{\partial z}\left[\frac{\mu_e}{\rho Pr_e}\frac{\partial}{\partial z}(\rho m_s)\right] \tag{8}$$

where a turbulent Lewis number of unity is assumed.

The turbulent viscosity and Prandtl number are obtained by solving conservation equations for k and ε. For horizontal buoyancy driven flows, such as turbulent thermal convection above a horizontal heated plate, the turbulence kinetic energy budget consists of molecular and turbulent diffusion, buoyant production and destruction, and dissipation [21]. If the flow is randomly three-dimensional, stress production is eliminated as a result of Reynolds averaging. If molecular diffusion is important, a low Reynolds number form of the k–ε model [22] must be chosen, and appropriate expressions for buoyant production and destruction [13] must be included.

In this study the following turbulence kinetic energy equation has been used

$$\frac{\partial k}{\partial t} = \frac{1}{\rho}\frac{\partial}{\partial z}\left[\left(\mu + \frac{\mu_t}{\sigma_k}\right)\frac{\partial k}{\partial z}\right] + \frac{g\mu_t}{\rho Pr_t}\left[\beta_s\frac{\partial(\rho m_s)}{\partial z} - \beta_T\frac{\partial T}{\partial z}\right] - \varepsilon - \frac{2\mu}{\rho}\left[\frac{\partial k^{1/2}}{\partial z}\right]^2 \tag{9}$$

where the first three terms on the RHS account for the effects of molecular and turbulent diffusion [22], buoyant production or destruction [13], and dissipation, respectively. The last term is empirical and is used in low turbulence Reynolds number k–ε models to account for the anisotropic component of the dissipation.

The conservation equation for the dissipation is of the form

$$\frac{\partial \varepsilon}{\partial t} = \frac{1}{\rho}\frac{\partial}{\partial z}\left[\left(\mu + \frac{\mu_t}{\sigma_\varepsilon}\right)\frac{\partial \varepsilon}{\partial z}\right] + c_{1\varepsilon}(1 - c_{3\varepsilon}) \times \frac{g\mu_t \varepsilon}{\rho Pr_t k}\left[\beta_s \frac{\partial(\rho m_s)}{\partial z} - \beta_T \frac{\partial T}{\partial z}\right] - f_2 c_{2\varepsilon}\varepsilon^2/k \quad (10)$$

where terms on the RHS account for molecular and turbulent diffusion, buoyant production or destruction, and viscous destruction. Equations (9) and (10) are solved throughout the bottom mixed layer and the overlying stable region. Since turbulence properties cannot be transported upward through the stable fluid, the molecular dynamic viscosity is included in the diffusion terms only if finite values of k or ε exist at a particular vertical location. As such, at the interfacial boundary layer represented mathematically by the control volume boundary separating grid nodes with nonzero and zero values of k and ε, turbulence properties are diffused from the mixed layer to the motionless ($k = \varepsilon = 0$) grid node. At the motionless node, the diffused turbulence properties are either destroyed by the stable density gradient or are sufficient to offset this gradient, thereby transforming this node from a motionless to a turbulent condition. It is this transformation which results in growth of the mixed layer.

The empirical function, f_2, is [22]

$$f_2 = 1.0 - 0.3\exp(-Re_t^2) \quad (11)$$

where the turbulence Reynolds number, Re_t, is

$$Re_t = \rho k^2/(\mu\varepsilon). \quad (12)$$

The turbulent viscosity depends on local values of k and ε [22]

$$\mu_t = c_\mu \exp[-2.5/(1 + Re_t/50)]\rho k^2/\varepsilon \quad (13)$$

where c_μ is an empirical constant. An expression for the turbulent Prandtl number is obtained from studies conducted in buoyant flows and is of the form [23]

$$Pr_t = \phi/\phi_t\left[\frac{1 + \phi_t'(c_t' - \phi_t)B}{1 + B\phi\phi_t}\right] \quad (14)$$

where ϕ, ϕ_t, ϕ_t', and c_t' are empirical constants and B is a buoyancy parameter defined as

$$B = g(k/\varepsilon)^2\left[\beta_T \frac{\partial T}{\partial z} - \beta_s \frac{\partial(\rho m_s)}{\partial z}\right]. \quad (15)$$

It should be noted that equation (14) was developed for single-diffusive buoyant flows. Its use in this study is due to the lack of analogous expressions for the double-diffusive case.

The coupled differential, (7)–(10), and algebraic, (11)–(15), equations constitute the mathematical model for the system of interest. Values of the empirical constants correspond to those commonly used in the literature ($c_{1\varepsilon} = 1.44$, $c_{2\varepsilon} = 1.92$, $c_{3\varepsilon} = 0.8$, $c_\mu = 0.09$, $c_t' = 1.6$, $\phi = 0.2$, $\phi_t = 0.31$, $\phi_t' = 0.155$, $\sigma_k = 1.0$, $\sigma_\varepsilon = 1.3$). Recently suggested revisions to the value of σ_k [18] were also considered, but the revisions resulted in only minor changes to the predicted quantities of interest.

Boundary conditions correspond to a prescribed heat flux at the bottom surface, which is impermeable and is characterized by $k = 0$. The top surface is adiabatic and impermeable and is characterized by $k = \varepsilon = 0$. At the first node adjacent to the bottom surface, ε depends on the bottom heat flux and the local turbulence kinetic energy. This dependence is obtained by assuming a negligible change in thermal energy storage for the half control volume adjacent to the heated surface and rearranging equation (7) to yield the following transcendental equation

$$\varepsilon = -\frac{(\phi_t \rho c_\mu k^2/\phi)}{(q_b/(c\,\partial T/\partial z) + \mu/Pr)} \times \exp[-2.5/(1 + \rho k^2/50\mu\varepsilon)]. \quad (16)$$

Use of equation (16) as a boundary condition for ε yields unique values for the dissipation which are consistent with the thermal and k boundary conditions. Efforts to use boundary conditions common to shear flows, such as equating local dissipation to production at the heated surface or prescribing a value of $\varepsilon = 0$ at the solid boundary, resulted in unrealistic predictions suggesting that conditions near the heated surface are inherently different and perhaps more complex for the system of interest.

The system of coupled differential and algebraic equations is solved by applying the transient, one-dimensional, finite-difference technique of Patankar [24]. Grid and time step halving techniques were used to determine values of Δz (≈ 1.8 mm) and Δt (≈ 1 s) required for stable system behavior. As an initial perturbation, the molecular viscosity was arbitrarily included in the coefficients of the buoyant production terms of equations (9) and (10) for the first few iterations. A CDC 6600 computational time of 1000 s was required to simulate 1 h of system behavior.

EXPERIMENTAL METHODS

To validate the model, a series of experiments were performed in which an initially isothermal, nearly linearly stratified solution was heated from below. The solution was contained in an acrylic test cell of square base (305 × 305 mm) and 200 mm height. Bottom heating was achieved by placing an electrical patch heater between a 1.6 mm copper plate (the bottom interior surface) and a 25 mm styrofoam sheet. A second patch heater was installed between the styrofoam and

additional insulation. The second heater was used as a guard and was controlled by the differential output of thermistors placed above and below the styrofoam sheet. The side walls of the test cell were insulated with 50 mm styrofoam insulation.

The test cell was filled with six layers of different salt concentration, and within two days diffusion provided for a nearly linear initial salt concentration profile throughout the 180 mm deep salt solution. Both an initial solution withdrawal/weight analysis technique and numerical analysis of the transient species diffusion equation showed that the linear salinity profile extended to within 10 mm of the impermeable boundaries, beyond which the profile smoothly changed to achieve a zero gradient at the boundaries.

Vertical temperture profile measurements were obtained by using a rake of 29 calibrated, copper–constantan thermocouples placed at 6.4 mm intervals. The rake was placed near the center of the test cell. An additional thermocouple was installed below the copper plate to monitor the heated surface temperature, and a fast (≈ 10 ms) response copper–constantan thermocouple was mounted from the end of a 1.5 mm traversable stainless-steel tube to measure fluctuating temperatures at various locations. All measurements and subsequent signal analysis were performed with a Hewlett–Packard 3054A data acquisition system. The sample rate for a 20 min burst of fluctuating temperature measurements was six readings per second. Average temperatures were determined by fitting a straight line through the entire temperature history obtained at a given vertical location, while probability density functions were calculated by summing the number of temperature samples bracketed by a specified range of T'.

Initial salt concentration profiles and mixed layer salt concentrations were obtained by withdrawing solution with a hypodermic needle whose tip was inserted normal to the gravitational vector. Subsequent weight analysis was performed on the extracted sample. Mixed layer heights were obtained by using the shadowgraph technique [11].

Table 1. Experimental conditions

Experiment	$(\partial m_s/\partial z)_i$	q_b	Ra_T^*/Ra_s	X
1	−30.0	40	0.067	1
2	−5.9	40	0.340	5
3	−5.9	90	0.770	11.5
4	−30.0	450	0.760	11.5
5	−19.0	450	1.200	18
6	−5.9	450	3.850	57

Six experiments were performed for different values of the initial salt concentration gradient and bottom heat flux. A relative stability parameter of the form

$$X_j = \frac{(Ra_T^*/Ra_s)_j}{(Ra_T^*/Ra_s)_{\min}} \tag{17}$$

may be associated with each of the j experiments, where the minimum Rayleigh number ratio corresponds to the first experiment ($j = 1$). Approximate values of initial salt concentration gradients, bottom heat flux, Rayleigh number ratio, and stability parameter are shown in Table 1.

RESULTS

Measured and predicted transient temperature profiles for the lower 120 mm of the 180 mm deep salt solution are shown in Fig. 2 for the six experiments. The top row of the figure reveals system behavior for the

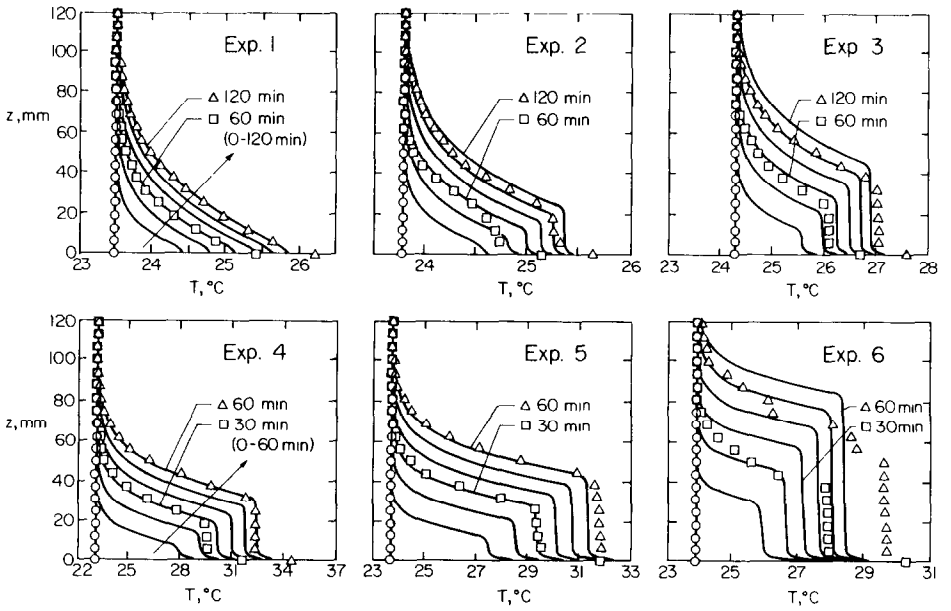

FIG. 2. Measured and predicted temperature distributions.

first 2 h of experiments 1–3, while the bottom row corresponds to the first hour of the remaining experiments. Since conditions of experiments 4–6 are less stable, the system responds more rapidly to the applied heat flux. Predicted temperatures are shown at 20 and 10 min intervals for experiments 1–3 and 4–6, respectively, while measured temperatures are shown at 60 and 30 min intervals to prevent cluttering of the figure.

A wide range of system response is revealed in Fig. 2. For example, the results of experiment 1 indicate the absence of mixed layer formation and vertical transport exclusively by diffusion. As X is increased, however, stronger thermal destabilization results in the formation of a single mixed layer (experiment 2). The mixed layer grows with time, while temperatures within the layer become more uniform due to local convective mixing. Heat loss to the diffusive region is significant, as revealed by the developing temperature profile in this region. Contrasting experiments 2 and 3, it is clear that the growth rate of the mixed layer increases with increasing X and that a uniform mixed layer temperature distribution is attained more quickly. Note that the mixed layer temperature is uniform in all but a thin thermal boundary layer at the bottom surface, from which the convective mixing originates. For different experimental conditions but identical values of X, the mixed layer heights of experiments 3 and 4 agree to within 15% at $t = 1$ h.

As X is increased further, shadowgraph results indicate formation of a secondary mixed layer above the bottom convecting region (experiment 5). However, the shadowgraphs suggest that mixing within the secondary layer is weak, and this observation is confirmed by the temperature measurements, which still indicate a nonuniform temperature distribution above the bottom mixed layer. For the highly unstable conditions of experiment 6, mixed layer growth is rapid and two secondary layers are formed. Measured temperatures within these layers are nearly uniform, suggesting the existence of vigorous mixing.

There is good agreement between the predicted and measured temperature distributions for all but experiment 6. The excellent agreement for experiment 1 is especially encouraging. Although weak mixing is predicted to occur directly above the bottom surface (as evidenced by the slight variation in the temperature gradient), the model confirms the existence of diffusion dominated conditions throughout the system. This result implies that the double-diffusive system will not experience convective motion if the Rayleigh number ratio is less than 0.067. In contrast other models [5, 7, 10, 12] would predict mixed layer development, when no such development is indicated by the data. Agreement for experiments 2–5 is also good, although the temperature of the heated surface is consistently underpredicted. Since the model is unable to predict the growth of secondary layers, there is poor agreement with the temperature profile data for experiment 6. However, the predicted density profiles at $t \approx 30$ min

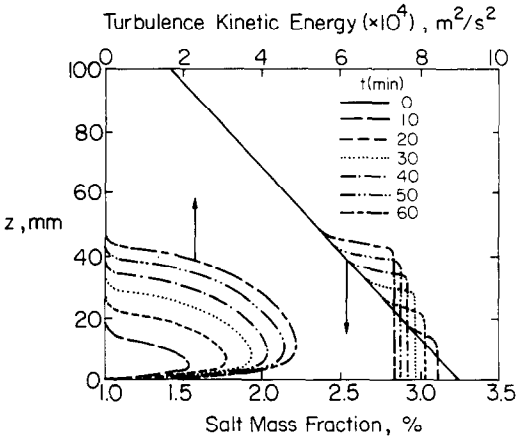

FIG. 3. Predicted salt mass fraction and turbulence kinetic energy distributions for experiment 5.

revealed unstable density distributions immediately above the bottom mixed layer. The shadowgraphs of experiment 6 also indicated the development of a secondary layer at this time. Unstable density distributions above the advancing mixed layer were not predicted for experiment 5 which, as previously noted, eventually developed a weak secondary layer.

Although Fig. 2 reveals good agreement between predicted and measured mixed layer heights, it should be noted that at later times (for example, at $t = 4$ h for experiment 3), the bottom mixed layer height is overpredicted by approximately 20%. This deficiency may be due to failure of the model to accurately represent mixing and entrainment processes and/or to changes in the nature of the mixing and the entrainment mechanism with increasing height. However, a meaningful comparison of measured and predicted temperature profiles at later times is compromised by the penetration of thermal effects to the upper surface and hence a breakdown in the model assumption of adiabatic conditions at this location. The lack of reliable heat and mass transfer correlations for the air/water interface precludes system prediction after thermal effects propagate to the upper surface.

In addition to the temperature distribution, the model also predicts vertical distributions of local quantities such as the salt concentration and turbulence kinetic energy. Representative results for experiment 5 are shown in Fig. 3. The salt concentration distribution remains unchanged in the diffusive region, while becoming uniform and decreasing with time in the mixed layer. This behavior is consistent with results obtained from a simpler, multi-layer model [10] and has been confirmed from limited measurements based on withdrawn solution samples.

The increasing salt concentration difference across the interfacial boundary layer is responsible for the decreasing growth rate of the mixed layer and strongly influences overall behavior of the double-diffusive system. The model predicts the s-shaped salinity distribution in the interfacial boundary layer which,

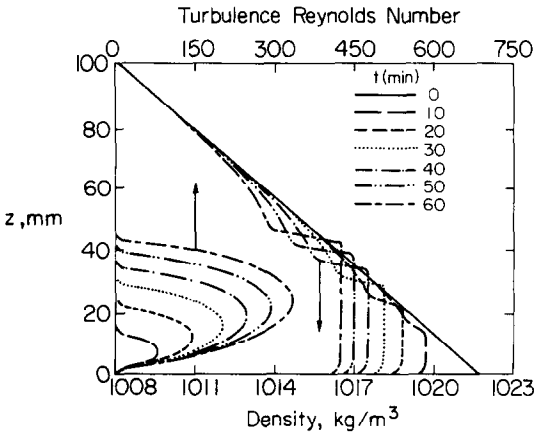

FIG. 4. Predicted density and turbulence Reynolds number distributions for experiment 5.

until now, could only be inferred by the use of shadowgraph [6] or interferometric [25] flow visualization techniques.

The turbulence kinetic energy distribution in the mixed layer indicates increasing energy with increasing time. Values of k are largest near the heated surface, which is the source of all convective motion, and decrease as the interfacial boundary layer is approached. Similar behavior has been observed in grid mixed salt-stratified solutions [26], where experimental horizontal root-mean-square (rms) velocities were also observed to decrease as the interfacial boundary layer was approached. Turbulence kinetic energy profiles predicted by applying a stress/flux model to the thermally stratified atmospheric boundary layer heated from below are also in qualitative agreement with those of Fig. 2 [15].

Figure 4 includes predicted density and turbulence Reynolds number distributions for experiment 5. The density profiles reveal a density inversion just above the heated surface, which drives the convective motion, and a large density difference across the interfacial boundary layer, which is due to the large salt concentration difference. The reduction in density which occurs above the interfacial boundary layer is due primarily to the developing temperature profiles shown in Fig. 1.

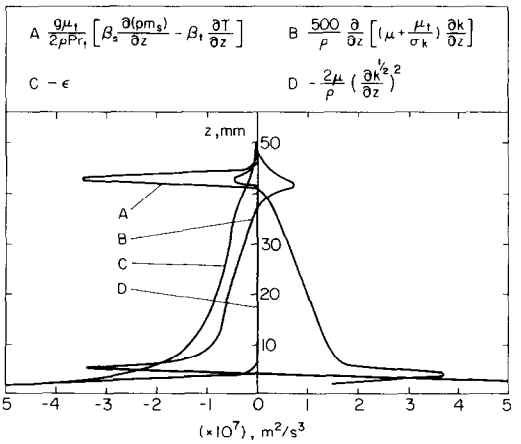

FIG. 5. Predicted turbulence kinetic energy budget for experiment 5, t = 1 h.

Turbulence Reynolds number distributions within the mixed layer are similar to the turbulence kinetic energy distributions of Fig. 3. The convecting fluid is characterized by low Reynolds numbers, especially near the heated surface and the interfacial boundary layer, thus affirming the selection of a low Reynolds number k–ε model.

The predicted turbulence kinetic energy budget is shown in Fig. 5 at t = 1 h for experiment 5. As expected, buoyant production (A) is most important directly above the heated surface and decreases gradually as the interfacial boundary layer is approached, at which point the term becomes negative and buoyant destruction is significant. Dissipation (C) exhibits a maximum directly above the heated surface and decreases as the interfacial boundary layer is approached. The ε profile is identical to results obtained by applying a stress/flux model to the thermally stratified atmospheric boundary layer heated from below [15]. The combined molecular and turbulent diffusion profile (B) indicates that turbulence kinetic energy is transported from the highly turbulent core of the mixed layer downward toward the heated surface and upward to the interfacial boundary layer, where it is consumed in an entrainment process.

Because the k–ε model is based on a gradient diffusion concept for which the turbulent diffusion of kinetic energy is assumed to be proportional to a local turbulence kinetic energy gradient, its application to buoyancy driven flows has been questioned. In particular Lumley *et al.* [14] have indicated that application of the model to thermally stratified systems heated from below is suspect, since the actual direction of transport of k may be locally opposite to the direction predicted by gradient diffusion. Specifically, the transport of turbulence from the highly turbulent central core of the mixed layer downward to the heated surface is also predicted for thermally stratified systems heated from below and is considered to be incorrect [14]. Since they conclude that a mixed layer powered by a gradient model 'cannot behave properly', the diffusional component of the turbulence kinetic energy budget merits special consideration. In particular, it is of interest to contrast the predicted distribution of this component with results associated with other physical systems.

Although the thermally stratified system heated from below [14] is similar to the double-diffusive system of this study, stable density differences associated with its interfacial boundary layer are much less than those of the double-diffusive system. As such, mixed layer growth is much more rapid [27]. In contrast, thermal convection between parallel horizontal plates involves a confined mixed layer for which no turbulent kinetic energy is expended in an entrainment process. Hence it is reasonable to speculate that the vertical distribution

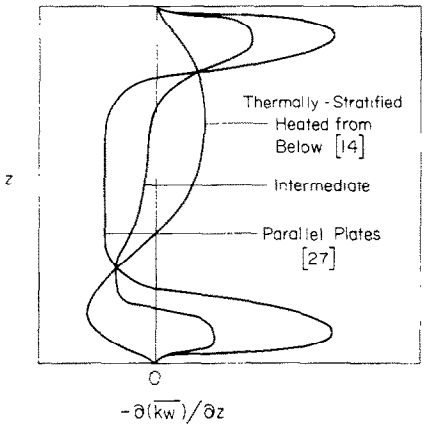

FIG. 6. Qualitative distributions of vertical turbulence kinetic energy flux for thermally stratified systems heated from below [14], parallel plates heated from below [27], and the intermediate case.

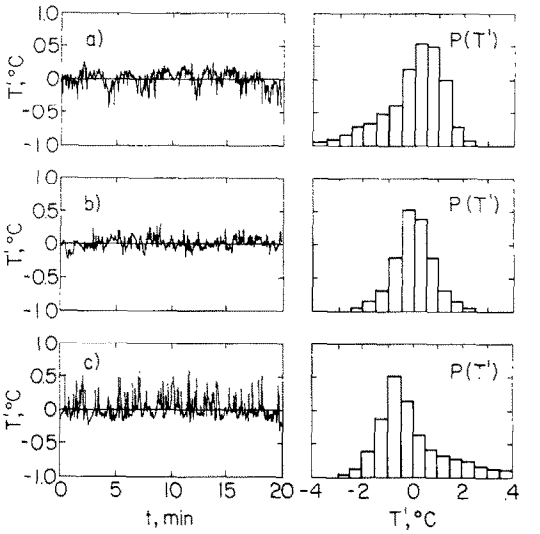

FIG. 7. Fluctuating temperature histories and the associated normalized probability density functions measured (a) below the interfacial boundary layer; (b) approximately mid-height in the mixed layer; and (c) above the heated surface for experiment 5.

of the turbulent diffusion flux in a double-diffusive mixed layer should be intermediate to distributions associated with the thermally stratified and horizontal plate conditions.

Qualitative distributions of the vertical turbulence kinetic energy flux are shown in Fig. 6 for the thermally stratified and parallel plate conditions. The distribution for the thermally stratified system is hypothetical [14], while that for the parallel plates is experimental [27]. The fact that the form of the intermediate distribution is similar to the predicted profiles of this study (for example, B, of Fig. 4) suggests that inclusion of the gradient diffusion concept in the k–ε model cannot be deemed inappropriate for salt-stratified, double-diffusive systems heated from below. However, verification of this concept must await detailed experimental measurements in systems of this nature.

The highly anisotropic dissipation predicted by the k–ε model (D of Fig. 5) is significant just above the heated surface and, to a lesser extent, directly below the interfacial boundary layer. Since dissipation scales are always more isotropic than energy scales [13], the turbulence kinetic energy should also be highly anisotropic at these locations. This trend is confirmed by fluctuating temperature histories measured at three locations (approximately 5 mm below the interfacial layer, at the center of the mixed layer, and 5 mm above the heated surface) during experiment 5 (Fig. 7). Since the system is thermally driven, it is reasonable to assume that velocity and temperature fluctuations are coupled at any location. Hence the downward temperature spikes of Fig. 7(a) may be associated with descending thermals containing high momentum, cool fluid. Conversely, the upward spikes of Fig. 7(c) are indicative of ascending thermals containing high momentum, warm fluid. Neither ascending nor descending thermals dominate motion in the middle of the mixed layer [Fig. 7(b)].

Normalized probability density functions corresponding to the temperature fluctuations are also shown in Fig. 7. Clearly, the fluctuating temperature record is highly anisotropic directly above the heated surface and near the interfacial boundary layer, while conditions in the middle of the mixed layer are essentially isotropic.

The model may also be tested by determining its compatibility with existing diffusive layer entrainment correlations. For double-diffusive systems, mixed layer growth rates may be normalized by the convective velocity

$$u_* = (g\beta_T q_b \delta/\rho c)^{1/3} \tag{18}$$

and correlated against the overall mixed layer Richardson number

$$Ri = g\Delta\rho\delta/(\rho u_*^2) \tag{19}$$

where $\Delta\rho$ is the stable density difference across the interfacial boundary layer. All thermophysical properties in equations (18) and (19) are evaluated at the salinity and temperature of the mixed layer. Analysis of experimental results obtained for long term (days) experiments conducted in larger test cells shows that the correlation governing mixed layer growth is [11]

$$u_e/u_* = 0.25\, Ri^{-1} \tag{20}$$

where u_e is the entrainment velocity or growth rate of the mixed layer.

Values of u_* and Ri have been computed from the model predictions for selected times (20-min intervals beginning at $t = 20$ min) corresponding to experiments 2–5. The results are well correlated by an exponent of -1 and a coefficient of 0.55, except for experiment 2 which was characterized by small mixed layer heights and slow growth rates, making it difficult to accurately

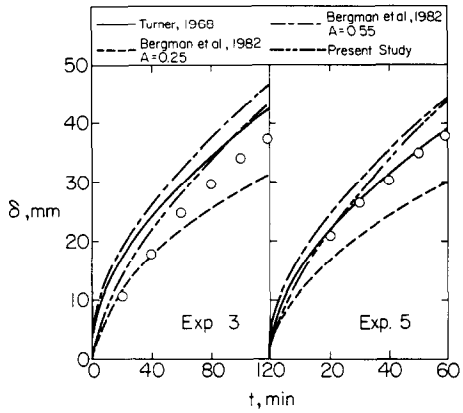

FIG. 8. Measured and predicted mixed layer heights for experiments 3 and 5.

determine required values of δ, u_e, and $\Delta\rho$. The exponent of the correlation does not deviate from the -1 value, although the coefficient varies by approximately $\pm 5\%$. Hence the model predicts the Richardson number dependence of equation (20) but consistently overpredicts the magnitude of the entrainment rate. This discrepancy may be due to failure of the model to include the actual entrainment mechanism or to the fact that entrainment phenomena associated with early mixed layer growth in small test cells and at small Richardson numbers ($50 < Ri < 300$) are inherently different from those associated with conditions for which equation (20) was developed (prolonged growth in larger test cells and Richardson numbers, $10^3 < Ri < 10^4$). Nevertheless, it is encouraging that the turbulence model is able to predict a major trend associated with mixed layer growth.

In Figs. 8 and 9, measured mixed layer heights and temperatures are compared with predictions based on the single layer model of Turner [7], the two-layer model of Bergman *et al.* [10], and the turbulence model of this study. Mixed layer heights (Fig. 8) predicted by the Turner and turbulence models are bracketed by results of the two-layer model and are in general agreement with the data. Success of the Turner model is surprising, in view of the large number of simplifying assumptions. However, this success does not extend to the mixed layer temperature (Fig. 9). Since the Turner model assumes negligible heat loss to the overlying diffusive region, mixed layer temperatures are significantly overpredicted. The two-layer model with an entrainment coefficient of 0.25 underpredicts mixed layer heights and overpredicts mixed layer temperatures. The opposite behavior characterizes use of $A = 0.55$, although there is some improvement in the agreement with data. The best overall agreement with data is provided by the turbulence model, although, as discussed previously, mixed layer heights are overpredicted at later times.

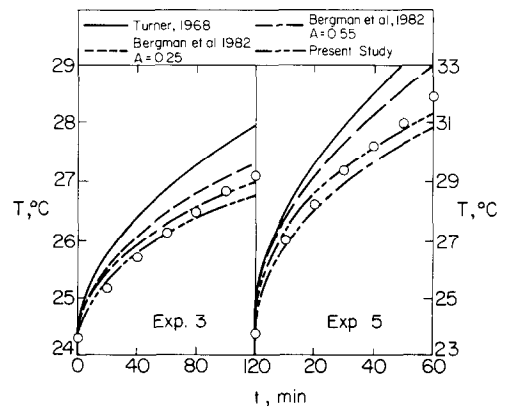

FIG. 9. Measured and predicted mixed layer temperatures for experiments 3 and 5.

SUMMARY

A differential turbulence model has been formulated to predict the response of a salt-stratified, double-diffusive system to heating from below. Model results are in good agreement with mixed layer growth and temperature data. Key features associated with systems of this nature have been predicted. For example, large salinity and density variations across the interfacial boundary layer have been shown to exist. Turbulence kinetic energy distributions within the convecting mixed layer have been predicted in conjunction with regions of anisotropic turbulence. Predicted distributions of buoyant production and destruction, isotropic dissipation, anisotropic dissipation, and diffusion are plausible, but cannot be confirmed due to the absence of appropriate experimental data. Although mixed layer growth rates are slightly overpredicted, the model yields the established dependence of growth rate on the Richardson number and is considered to perform as well or better than previous models.

Acknowledgement—Support of this work by the National Science Foundation under Grant No. MEA-8316580 is gratefully acknowledged.

REFERENCES

1. J. S. Turner, *Buoyancy Effects in Fluids.* Cambridge University Press, Cambridge (1979).
2. H. Tabor, Solar ponds, *Solar Energy* **27,** 181–194 (1981).
3. M. Morioka and S. Enya, Natural convection of density-stratified layers in a vessel I: Observation of flow patterns, *Heat Transfer Jap. Res.* **12,** 48–69 (1983).
4. S. Ostrach, Fluid mechanics of crystal growth—the 1982 Freeman Scholar Lecture, *Trans. Am. Soc. Mech. Engrs,* Series I, *J. Fluids Engng* **105,** 5–20 (1983).
5. H. E. Huppert and P. F. Linden, On heating a stable salinity gradient from below, *J. Fluid Mech.* **95,** 431–464 (1979).
6. C. J. Poplawsky, F. P. Incropera, and R. Viskanta, Mixed layer development in a double-diffusive thermohaline system, *Trans. Am. Soc. Mech. Engrs,* Series J, *J. Solar Energy Engng.* **103** 351–359 (1981).
7. J. S. Turner, The behavior of a stable salinity gradient heated from below, *J. Fluid Mech.* **33,** 183–200 (1968).
8. C. J. Poplawsky, Laboratory simulation of the solar pond, double-diffusive, thermohaline system, M.S. thesis, Purdue University, W. Lafayette, Indiana (1980).

9. J. S. Turner, The coupled turbulent transports of salt and heat across a sharp density interface, *Int. J. Heat Mass Transfer* **8**, 759–767 (1965).
10. T. L. Bergman, F. P. Incropera, and R. Viskanta, A multilayer model for mixing layer development in a double-diffusive thermohaline system heated from below, *Int. J. Heat Mass Transfer* **25**, 1411–1418 (1982).
11. T. L. Bergman, D. R. Munoz, F. P. Incropera, and R. Viskanta, Correlation for entrainment of salt-stratified fluid by a thermally driven mixed layer, *Am. Soc. Mech. Engrs.* Paper No. 83-WA/HT-76 (1983).
12. K. A. Meyer, A one-dimensional model of the dynamic layer in a salt gradient solar pond, *Proc. Conf. American Section Int. Solar Energy Soc.*, pp. 763–767 (1981).
13. W. Rodi, *Turbulence Models and Their Application in Hydraulics: A State of the Art Review*. University of Karlsruhe, Federal Republic of Germany (1980).
14. J. L. Lumley, O. Zeman, and J. Seiss, The influence of buoyancy on turbulent transport, *J. Fluid Mech.* **84**, 581–597 (1978).
15. O. Zeman and J. L. Lumley, Modeling buoyancy driven mixed layers, *J. Atmos. Sci.* **33**, 1974–1988 (1976).
16. J. C. Wyngaard, The atmospheric boundary layer-modeling and measurements, *Proc. Conf. Second Symposium on Turbulent Shear Flow*, Imperial College, pp. 13.25–13.30 (1979).
17. J. W. Deardorff, The use of subgrid transport equations in a three-dimensional model of atmospheric turbulence, *Trans. Am. Soc. Mech. Engrs*, Series I, *J. Fluids Engng* **95**, 429–438 (1973).
18. A. A. Sonin, Calibration of the k–ε turbulence model for the diffusion of turbulence, *Phys. Fluids* **26**, 2769 (1983).
19. D. R. Caldwell, Thermal and Fickian diffusion of sodium chloride in a solution of oceanic concentration, *Deep-Sea Res.* **20**, 1029–1039 (1973).
20. United States Office of Saline Water, Technical Data Book (1964).
21. A. A. Townsend, *The Structure of Turbulent Shear Flow*. Cambridge University Press, Cambridge (1976).
22. W. P. Jones and B. E. Launder, The prediction of laminarization with a two-equation model of turbulence, *Int. J. Heat Mass Transfer* **15**, 301–304 (1972).
23. M. M. Gibson and B. E. Launder, On the calculation of horizontal, turbulent, free shear flows under gravitational influence, *Trans. Am. Soc. Mech. Engrs*, Series C, *J. Heat Transfer* **98**, 81–87 (1976).
24. S. V. Patankar, *Numerical Heat Transfer and Fluid Flow*. McGraw-Hill, New York (1980).
25. W. T. Lewis, F. P. Incropera, and R. Viskanta, Interferometric study of stable salinity gradients heated from below or cooled from above, *J. Fluid Mech.* **116**, 411–430 (1982).
26. S. M. Thompson and J. S. Turner, Mixing across an interface due to turbulence generated by an oscillating grid, *J. Fluid Mech.* **67**, 349–368 (1975).
27. J. W. Deardorff, G. E. Willis and B. H. Stockton, Laboratory studies of the entrainment zone of a convectively mixed layer, *J. Fluid Mech.* **100**, 41–64 (1980).
28. J. W. Deardorff and G. E. Willis, Investigation of turbulent thermal convection between horizontal plates, *J. Fluid Mech.* **28**, 675–704 (1967).

UN MODELE DIFFERENTIEL POUR DES SYSTEMES STRATIFIES EN SALINITE, DOUBLEMENT DIFFUSIFS ET CHAUFFES PAR LE BAS

Résumé—On présente un modèle différentiel et on l'utilise pour calculer la réponse transitoire d'un système stratifié en salinité, doublement diffusif et chauffé par le bas. Les hauteurs de couche de mélange et les distributions de température calculées sont en bon accord avec les données et en accord raisonnable avec des modèles à une et deux couches. Les particularités du système telles que la différence de densité à travers la couche limite interfaciale, la variation négligeable du profil de salinité dans la région stable et les régions de mouvement fortement anisotrope du fluide, sont bien décrites par le modèle. Les caractéristiques calculées de la turbulence sont plausibles et les vitesses de croissance de la couche de mélange sont cohérentes avec les formules acceptées contenant une vitesse convective et un nombre de Richardson pour la couche de mélange.

EIN DIFFERENZENMODELL FÜR SYSTEME AUS SALZSCHICHTEN, DIE VON UNTEN BEHEIZT WERDEN

Zusammenfassung—Ein Differenzenmodell wurde entwickelt und dazu verwendet, um das instationäre Verhalten eines salzgeschichteten 'doppelt-diffusiven' Systems zu berechnen, das von unten beheizt wird. Die berechnete Höhe der Mischungsschicht und die Temperaturverteilung sind in guter Übereinstimmung mit Ergebnissen und in annehmbarer Übereinstimmung mit Berechnungen, welche mit einfacheren Ein- und Zweischichtmodellen durchgeführt wurden. Die Hauptkennzeichen des Systems wie der maßgebliche Dichteunterschied über die Grenzschicht, die vernachlässigbare Änderung des Salzgehalt-Profils in den stabilen Abschnitten und die Gebiete von stark anisotroper Fluidbewegung werden durch das Modell gut beschrieben. Die berechneten Turbulenzcharakteristiken sind einleuchtend, und die berechneten Wachstumsraten der Mischschicht sind mit anerkannten Korrelationen vereinbar, welche eine Konvektionsgeschwindigkeit und eine Richardson-Zahl für die Mischschicht enthalten.

РАЗНОСТНАЯ МОДЕЛЬ НАГРЕВАЕМЫХ СНИЗУ ДВУХДИФФУЗИОННЫХ СИСТЕМ С СОЛЕВОЙ СТРАТИФИКАЦИЕЙ

Аннотация—Разработанная разностная модель используется для расчета переходных характеристик нагреваемой снизу двухдиффузионной системы с солевой стратификацией. Рассчитанные высоты слоя смешения и распределения температуры хорошо согласуются с результатами, полученными на более простых одно- и двухслойных моделях. Определяющие характеристики системы, такие, например, как существенная разница плотности поперек пограничного слоя, пренебрежимо малое изменение профиля солености в устойчивой зоне и участки движения сильно анизотропной жидкости, хорошо описываются данной моделью. Рассчитанные характеристики турбулентности близки к реальным, а полученная скорость роста слоя смешения соответствует соотношениям, включающим конвективную скорость и число Ричардсона для слоя смешения.